Regular Article

Roland Tolulope Loto*

Effect of heat-treatment processes and high temperature variation of acid-chloride media on the corrosion resistance of B265 (Ti–6Al–4V) titanium alloy in acid-chloride solution

https://doi.org/10.1515/eng-2022-0037
received November 20, 2021; accepted February 01, 2022

Abstract: Corrosion resistance of untreated (B265TiN), quenched (B265TiQ), and annealed (B265TiA) B265 titanium alloy was studied in 2–10 M H_2SO_4 + 10% NaCl solution at 30, 70, and 95°C by potentiodynamic polarization, potentiostatic measurement, open circuit potential measurement, and optical microscopy. B265TiN was the most resistant of the alloys to general corrosion at 30°C with values between 0.094 and 3.782 mm/year. B265TiQ exhibited the highest corrosion rate values (0.210–23.399 mm/year). Its plots show significant increase in cathodic slope. At 70 and 95°C, B265TiN exhibited the lowest corrosion rate in 2 and 6 M H_2SO_4 + 10% NaCl solution, while B265TiQ exhibited the corresponding highest values. Optical characterization shows B265TiN, B265TiQ, and B265TiA alloys are highly resistant to corrosion in 2 M H_2SO_4 + 10% NaCl at 30°C compared to 10 M H_2SO_4 + 10% NaCl, where marginal deterioration occurred on B265TiN, significant degradation on B265TiQ, and localized degradation on B265TiA. The extent of degradation increased at 70 and 95°C. B265TiN exhibited the highest resistance to metastable pits formation compared to B265TiQ and B265TiA. Potentiostatic values at 70°C shows high temperature exposure of Ti alloy to accelerated corrosion. Metastable pit initiation values at 70°C are significantly greater. Open circuit potential measurement at 30°C shows B265TiN demonstrated least vulnerability to corrosion with stable oxide formation at 2 M and 6 M H_2SO_4 + 10% NaCl, and B265TiQ was least vulnerable at 10 M H_2SO_4 + 10% NaCl. At 70°C, B265TiQ was least vulnerable to corrosion with unstable oxide formation at 2 M and 6 M H_2SO_4 + 10% NaCl compared to B265TiN at 10 M H_2SO_4 + 10% NaCl.

Keywords: titanium, corrosion, acid-chloride, heat-treatment, pitting, passivation

1 Introduction

Titanium is a nonmagnetic low-density (60% of stainless steel density) alloy with excellent heat conduction properties. Its coefficient of thermal expansion is below that of steel and aluminum. The mechanical properties of titanium can be significantly modified through alloying and other manufacturing processes [1]. Their melting points are higher than those of steels, but the optimal relevant temperature range for structural applications is as low as 400°C to about 600°C with respect to composition. Mechanical properties are the primary performance characteristic for titanium applications. Biocompatibility is the most important factor in medicine. However, in industry, corrosion resistance is the most important requirement. Though the economic consequence for use of titanium alloys is (a) higher than ferrous and non-ferrous alloys in the short term, (b) the long-term operational cost is lower, and (c) the productive lifespan and service reliability are longer coupled with marginal maintenance cost. Increased metallic production capacity and efficiency, more efficient processing technologies, extensive market base, and unlimited demand have significantly lowered the cost of titanium alloys [2]. Titanium alloys are extensively utilized in aviation, chemical manufacturing [3–5], pharmaceutical [6–12], petrochemical [13,14], desalination, nuclear and energy generation, heat exchangers, geothermal [15], mining, and biomedical industries [16–18]. Titanium exhibits higher corrosion resistance than stainless steels in neutral chloride and oxidizing acid conditions. The corrosion resistance of titanium is on account of a stable

* **Corresponding author: Roland Tolulope Loto,** Department of Mechanical Engineering, Covenant University, Ota, Ogun State, Nigeria, e-mail: tolu.loto@gmail.com

and protective resistant oxide film whose nature strongly depends on environmental factors. The protective oxide evolves instantaneously on titanium surface when exposed to aqueous conditions [19–33]. The oxide remains resistive to general and localized corrosion in most oxidizing and neutral conditions without the need for corrosion inhibitors like ferrous and aluminum alloys though they are vulnerable in reducing media [34,35]. This can be mitigated through coating of the titanium alloy. Research on the corrosion study of laser cladded Ti–6Al–4V alloy in dilute NaCl, H_2SO_4 and HCl solutions showed that the coating displayed a more noble corrosion behavior compared to the untreated alloy [36]. They have weak corrosion resistance in acidified fluids [37–41]. Generally, the oxide is in the form of TiO_2, though it consists of other precipitates of titanium oxides at the metal interface (TiO_2, Ti_2O_3, and TiO) [42,43].

High-temperature application of titanium alloys tends to advance the evolution of a chemically stable, resistant, and crystalline covering of TiO. Titanium alloys are utilized as the liner and interior components of steam sterilizers during the high-pressure and temperature acid filtration of nickel laterite ores where they are prone to astringent conditions of acidity, temperature, and pressure [44]. Ti–6Al–2Sn–4Zr–2Mo alloy proves to be more corrosion resistant than Ti–6Al–4V [45]. Yang et al. [46] studied the effect of solution and aging treatments on the microstructure and the corrosion resistance of laser solid formed Ti–6Al–4V titanium alloy and found that aging treated Ti–6Al–4V showed corrosion resistance in 3.5 wt% NaCl solution showed corrosion resistance which was slightly better than the as-deposited Ti–6Al–4V. Rotating parts in jet-engine blades and gas turbine are currently made of titanium alloys which combine high strength and stable metallurgical structure for high temperature performance. Titanium alloys exhibit good potential for high temperature utilization in turbine parts owing to their good oxidation properties [47–51]. The corrosion behaviors of titanium alloy in high temperature applications vary with environments. In extractive metallurgy, titanium alloys are subjected to the deprecating action of reducing acids. According to Yue et al. [52], B265 titanium alloy reacted poorly in high Cl^- solution concentration and acidic environments containing Cl^- ions. Blanco-Pinzon et al. [53] stated that B265 titanium alloy was vulnerable to corrosion in H_2SO_4 solution in the absence of alloying elements of Pd and Ni. High temperature usage of titanium alloys in reducing environments subjects them to operating conditions which modify the physical, mechanical, and metallurgical properties, and strongly influences their corrosion resistance. Increased use of Ti alloys in extractive metallurgy and other high temperature applications has prompted research into their corrosion resistance properties in sulfuric acid solutions. B265 titanium is the most applicable titanium alloy among the αβ titanium alloys. Its corrosion resistance in HCl, H_2SO_4 and NaCl media at room and elevated temperatures from different production and manufacturing techniques have been researched into by other authors [54–64]. In contribution to the study of corrosion resistance of titanium alloys, this article studies the effect of heat-treatment processes and high temperature variation of acid-chloride media on the corrosion resistance of B265 (Ti–6Al–4V) titanium alloy.

2 Experimental methods

2.1 Materials preparation

B265 titanium alloy (B265TiN) obtained from the University of Johannesburg, Johannesburg, South Africa was analyzed with Phenom ProX Scanning Electron Microscope (Model No. MVE0224651193) at the Central Laboratory, Covenant University. The nominal (wt%) content of B265TiN alloy is shown in Table 1. B265TiN was cut by using a hacksaw into 15 specimens with dimensions of 1 cm × 1 cm × 0.5 cm (length × breadth × thickness). A total of 10 B265TiN specimens underwent annealing and quenching heat treatment process in a muffle furnace after heating the steel to 600°C and maintained at that temperature for 30 min. Annealed B265TiN (B265TiA) was gradually chilled in air, while quenched B265TiN (B265TiQ) was chilled in deionized H_2O. The temperature within the muffle furnace was sustained with a control dial at accuracy ±10°C and connected to a thermocouple (K-Type). A Cu wire was attached to B265TiN, B265TiQ, and B265TiA specimens with soldering iron, and the specimens were embedded in pre-hardened acrylic resin

Table 1: Nominal (wt%) constituent of B265 titanium alloy

Element	V	Al	Fe	O	C	N	H	Y	Ti
% composition	4	6	0.3	0.2	0.08	0.05	0.015	0.005	89.35

mounts. The exposed area of the embedded specimens (1 cm × 1 cm) were thereafter grinded with emery paper with 80, 120, 220, 600, and 1,000 grit sizes according to ASTMG59-97 [65]. B265TiN was then burnished with 6 µm diamond polishing solution and later sanitized with deionized H_2O and C_3H_6O in accordance with ASTM G1-03 [66].

2.2 Test solution

Standard grade recrystallized NaCl (obtained from Loba Chemie Pvt. Ltd, India) was prepared into volume concentrations of 10% in 400 mL of 2, 4, 6, 8, and 10 M H_2SO_4 solution by adding 40 g NaCl into a beaker and filling up to 400 mL of the required dilute H_2SO_4 solution concentration. Dilute H_2SO_4 was prepared from conventional grade reagent of the acid (98%, purchased from Sigma-Aldrich, USA).

2.3 Electrochemical test

Potentiodynamic polarization tests were performed at 30, 70, and 95°C with a ternary electrode configuration (working electrode, Ag/AgCl reference electrode, and Pt wire counter electrode) within a transparent beaker containing the acid-chloride electrolyte (placed on a portable heating device) using Digi-Ivy 2311 electrochemical workstation (plugged to a computer). Fisherbrand accumet glass body Ag/AgCl reference electrode was used for high temperature electrochemical test. The temperature of the heating device was thermostatically controlled. Polarization curves were drawn at sweep rate of 0.0015 V/s from −1.4 to +0.75 V according to ASTM G102-89(2015) [67]. Corrosion current density (C_D, A/cm^2) and corrosion potential (C_P, V) values were determined by the Tafel extrapolation method. Corrosion rate (C_R) was computed from the equation below:

$$C_R = \frac{0.00327 \star C_D \star E_Q}{D}, \quad (1)$$

where E_Q represents the specimen equivalent weight (g). 0.00327 represents constant for corrosion rate calculation in mm/year [68]. Open circuit potential measurement (OCP) was executed at 0.05 V/s step potential for 3,000 s to analyze the active-passive transition behavior and the thermodynamic stability of B265TiN, B265TiQ, and B265TiA alloys in 2 M H_2SO_4 + 10% NaCl, 6 M H_2SO_4 + 10% NaCl, and 10 M H_2SO_4 + 10% NaCl solutions at 30 and 70°C [69].

2.4 Optical microscopy characterization

Optical representative images of B265TiN, B265TiQ, and B265TiA alloy surfaces in 2 M H_2SO_4 + 10% NaCl and 10 M H_2SO_4 + 10% NaCl solutions at 30°C, 2 M H_2SO_4 + 10% NaCl and 6 M H_2SO_4 + 10% NaCl solutions at 70°C, and 2 M H_2SO_4 + 10% NaCl and 6 M H_2SO_4 + 10% NaCl solutions at 95°C were studied and compared using Omax microscope.

3 Results and discussion

3.1 Potentiodynamic polarization studies

Corrosion resistance of B265TiN, B265TiQ, and B265TiA titanium alloys were studied by potentiodynamic polarization method at 30°C. Potentiodynamic plots of B265TiN, B265TiQ, and B265TiA corrosion in 2, 4, 6, 8, and 10 M H_2SO_4 solution at 10% NaCl concentration are displayed in Figure 1(a)–(c). Table 2 shows the polarization data retrieved from the plots for B265TiN, B265TiQ, and B265TiA alloys. Data for B265TiN in Table 2 shows that increase in H_2SO_4 concentration results in proportionate increase in B265TiN corrosion. Corrosion rate of B265TiN in 2 M H_2SO_4 + 10% NaCl concentration is 0.094 mm/year which corresponds to corrosion current density of 8.07 × 10^{-6} A/cm^2 and polarization resistance of 3,184 Ω. B265TiN Corrosion rate value from 2–6 M H_2SO_4 + 10% NaCl concentration are well below 1 mm/year signifying strong resistance of B265TiN to corrosion within the acid-chloride media. The reaction of B265TiN in the electrolyte generally proceeds according to equation (2), where B265TiN alloy is oxidized to Ti^{3+} and passes into the electrolyte. Simultaneously, electrolytic transport of H^+ ions from the electrolyte to the metal exterior occurs leading to the formation of atomic hydrogen and subsequently H_2 gas according to equation (3) below;

$$Ti^{\circ} \rightarrow Ti^{3+} + 3e^{-} \text{ (anodic reaction)}, \quad (2)$$

$$2H^{+} \rightarrow 2\,H - 2e^{-} \rightarrow H_2 - 2e^{-} \text{ (cathodic reaction)}. \quad (3)$$

Corrosion resistance of B265TiN is primarily on account of the evolution of TiO_2 on the alloy surface [70,71], according to the equation (4). B265TiN reacts with

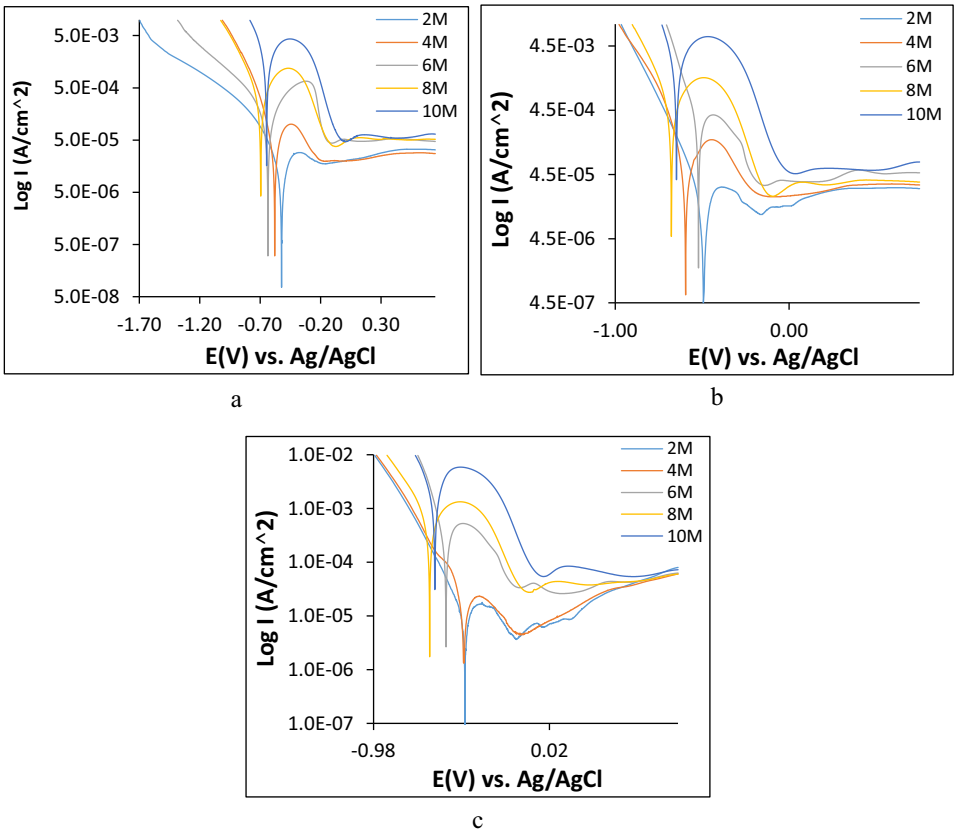

Figure 1: Potentiodynamic plots of (a) B265TiN, (b) B265TiQ, and B265TiA alloys in 2–10 M H_2SO_4 solution at 10% NaCl concentration.

Table 2: Potentiodynamic polarization output for B265TiN, B265TiQ, and B265TiA in 2–10 M H_2SO_4 + 10% NaCl at 30°C

Specimen	H_2SO_4 Conc. (M)/ 10% NaCl	B265 Corrosion rate (mm/year)	Corrosion current (A)	Corrosion current density (A/cm^2)	Corrosion potential (V)	Polarization resistance, R_p (Ω)	Cathodic potential, B_c	Anodic potential, B_a
B265TiN								
A	2	0.094	8.07×10^{-6}	8.07×10^{-6}	−0.523	3184.00	−6.92	4.327
B	4	0.350	3.02×10^{-5}	3.02×10^{-5}	−0.580	851.10	−9.74	4.079
C	6	0.760	6.55×10^{-5}	6.55×10^{-5}	−0.640	392.30	−6.048	5.782
D	8	2.390	2.06×10^{-4}	2.06×10^{-4}	−0.699	124.70	−6.941	5.237
E	10	13.782	1.19×10^{-3}	1.19×10^{-3}	−0.647	21.63	−7.184	4.408
B265TiQ								
A	2	0.210	1.81×10^{-5}	1.81×10^{-5}	−0.491	2097.00	−8.009	2.148
B	4	0.569	4.91×10^{-5}	4.91×10^{-5}	−0.595	523.30	−9.568	4.933
C	6	4.452	3.84×10^{-4}	3.84×10^{-4}	−0.524	66.94	−5.448	4.630
D	8	4.618	3.98×10^{-4}	3.98×10^{-4}	−0.677	64.54	−7.238	4.419
E	10	23.399	2.02×10^{-3}	2.02×10^{-3}	−0.648	12.74	−7.848	4.150
B265TiA								
A	2	0.135	1.16×10^{-5}	1.16×10^{-5}	−0.461	2211.00	−6.905	1.140
B	4	0.443	3.82×10^{-5}	3.82×10^{-5}	−0.467	695.00	−6.54	1.075
C	6	3.336	2.88×10^{-4}	2.88×10^{-4}	−0.568	89.33	−11.980	1.429
D	8	4.726	4.07×10^{-4}	4.07×10^{-4}	−0.661	63.06	−6.951	4.063
E	10	18.735	1.62×10^{-3}	1.62×10^{-3}	−0.631	15.91	−8.141	4.091

dissolved O_2 to produce the strong adherent oxide layer on its surface.

$$Ti + O_2 \rightarrow TiO_2. \quad (4)$$

Corrosion rate of B265TiN at 8 M H_2SO_4 + 10% NaCl concentration is 2.390 mm/year, while at 10 M H_2SO_4 + 10% NaCl concentration, B265TiN underwent severe surface deterioration with corrosion rate output of 13.782 mm/year. This value correlates with corrosion current density of 1.19×10^{-3} and polarization resistance of 21.63 Ω. The significantly low polarization resistance value at 2 M H_2SO_4 + 10% NaCl concentration in contrast to the extremely high value at 10 M H_2SO_4 + 10% NaCl concentration is an indication of the extent to which the TiO_2 formed on B265TiN alloy has thinned out and got damaged from the constant attack of the anionic species [72]. Observation of the cathodic portion of the polarization plots in Figure 1(a) exhibits significant increase in cathodic polarization slope and decrease in cathodic reaction time due to accelerated H_2 evolution and O_2 reduction reactions. The corrosion potential shift of the combined anodic-cathodic polarization plots shows that the corrosion reaction mechanisms are dominated by cathodic processes. This observation stems from the increase in SO_4^{2-} anionic concentration whose reaction (equation (5)) in conjunction with the presence of Cl^- anions (equation (6)–(13)) tends to breakdown TiO_2 protective film while simultaneously hindering its formation due to the occurrence of complex chemical precipitates. TiO_2 on B265TiN reacts with NaCl and O_2 (equations (6)–(8)) [73] as follows (equation (6)–(13));

$$2Ti + 3H_2SO_4 \rightarrow Ti_2(SO_4)_3 + 3H_2, \quad (5)$$

$$5TiO_2 + 4NaCl + O_2 \rightarrow Na_4Ti_5O_{12} + 2Cl_2, \quad (6)$$

$$6TiO_2 + 4NaCl \rightarrow Na_4Ti_5O_{12} + TiCl_4. \quad (7)$$

The Cl_2 in equation (5) transports through breakages on TiO_2 and reacts with the substrate B265TiN [74,75]. Cl^- anions contribute to the breakdown of the protective oxide (equations (6) and (11)). The greater reactivity of HCl compared to Cl_2 ensures accelerated deterioration of the alloy surface, thus, more substrate metal is consumed and released into the solution, resulting in higher corrosion rate.

$$5TiO_2 + 4NaCl + 2H_2O \rightarrow Na_4Ti_5O_{12} + 4HCl, \quad (8)$$

$$TiCl_4 + 2H_2O \rightarrow TiO_2 + 4HCl, \quad (9)$$

$$2HCl + Ti \rightarrow TiCl_2 + H_2, \quad (10)$$

$$4HCl + Ti \rightarrow TiCl_4 + 2H_2, \quad (11)$$

$$2TiCl_2 + O_2 + 2H_2O \rightarrow 2TiO_2 + 4HCl, \quad (12)$$

$$2H_2 + O_2 \rightarrow 2H_2O. \quad (13)$$

Quenching and annealing heat-treatment strongly influence the microstructure and metallurgical properties of B265TiN alloy which in effect influences the corrosion resistance of the alloy [76–79]. Heat-treatment had marginal influence on the general corrosion resistance of B265TiQ and B265TiA at 2 M and 4 M H_2SO_4 + 10% NaCl concentrations. Corrosion rate increased to 0.210 and 0.569 mm/year for B265TiQ, and 0.135 and 0.443 mm/year for B265TiA. At 6 M and 8 M H_2SO_4 + 10% NaCl concentrations, the margin of difference in corrosion rate for B265TiQ and B265TiA has increased further, compared to the corresponding value for B265TiN. Heat-treatment strongly influences the properties and strength of TiO_2 formed on B265TiQ and B265TiA alloys which invariably influences their interaction with anionic species from the electrolyte [80]. At 10 M H_2SO_4 + 10% NaCl concentration, corrosion rate of B265TiQ and B265TiA alloys culminated at 23.399 and 18.735 mm/year compared to 13.782 mm/year for B265TiN. The slopes of the cathodic reaction mechanisms for B265TiQ and B265TiA (Figure 1b and c) are significantly higher than the corresponding slopes for B265TiN (Figure 1a) due to increased cathodic reaction mechanisms during potential scanning. Corrosion potential of the heat-treated alloys is substantially influenced by the strength of the protective oxide [81]. The corrosion potential of the potentiodynamic plots for B265TiA shifted to lower potential due to dominant cathodic reaction process compared to the corresponding values for B265TiQ. The redox reaction mechanism counterbalanced each other for B265TiQ with respect to variation in H_2SO_4 concentration, while the corrosion potentials of B265TiA were marginally lower than the values for B265TiN.

Corrosion resistance of B265TiN, B265TiQ, and B265TiA alloys were further subjected to analysis in hot acid-chloride media (2 M and 6 M H_2SO_4 + 10% NaCl concentration) at 70 and 95°C. Figure 2a–c shows the potentiodynamic polarization plots of the anodic-cathodic reaction mechanisms of B265TiN, B265TiQ, and B265TiA alloys in 2 M and 6 M H_2SO_4 + 10% NaCl concentration at 70°C, while Figure 3a and b shows the corresponding polarization plots at 95°C. Tables 3 and 4 show the polarization data obtained at 70 and 95°C. Observation of Table 3 shows B265TiN exhibited the lowest corrosion rate values at 70°C for all the acid-chloride concentrations studied with values of 4.979 and 16.090 mm/year. Corrosion potential of the polarization plots for B265TiN in Figure 2a shifted from −0.516 V (2 M H_2SO_4 + 10% NaCl) to −0.566 V in Figure 3a (6 M H_2SO_4 + 10% NaCl) due to increased destruction of TiO_2 on its surface and dominant cathodic processes.

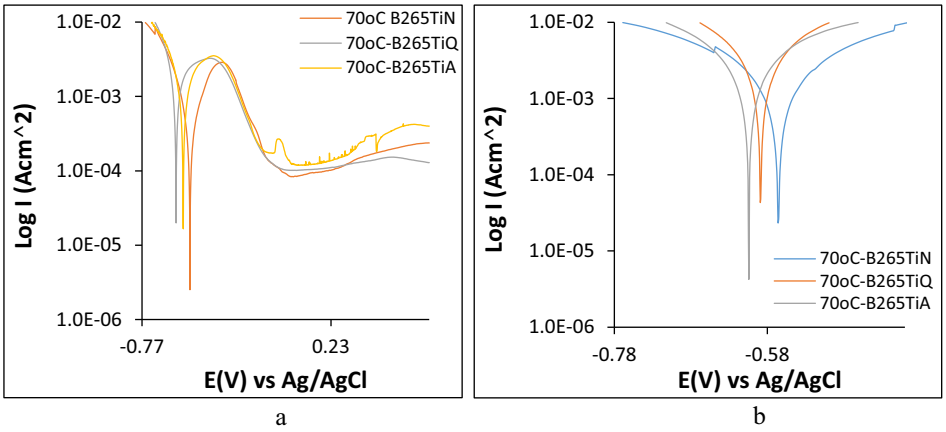

Figure 2: Potentiodynamic plots of B265TiN, B265TiQ, and B265TiA corrosion in (a) 2 M H_2SO_4 + 10% NaCl at 70°C and (b) 6 M H_2SO_4 + 10% NaCl at 70°C.

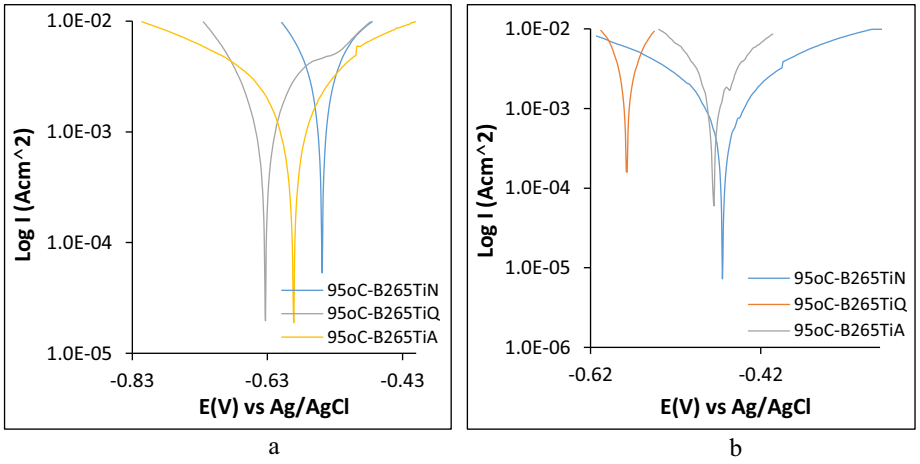

Figure 3: Potentiodynamic plots of B265TiN, B265TiQ, and B265TiA corrosion in (a) 2 M H_2SO_4 + 10% NaCl at 95°C and (b) 6 M H_2SO_4 + 10% NaCl at 95°C.

The polarization resistance of B265TiN (at 2 M and 6 M H_2SO_4 + 10% NaCl) are 59.87 and 18.52 Ω, respectively, which is a strong indication of the corrosion resistance properties of the protective oxide. B265TiQ exhibited the highest corrosion rates with corresponding values of 17.912 and 35.812 mm/year at polarization resistance of 16.64 and 8.32 Ω. Change in corrosion potential of the polarization plots (Figures 2b and 3b) with respect to electrolyte concentration was marginal from −0.585 to −0.589 V in the cathodic direction. At 95°C, corrosion rate of B265TiN, B265TiQ, and B265TiA in 2 M H_2SO_4 + 10% NaCl media visibly increased to 11.937, 20.824, and 15.302 mm/year compared to their values at 70°C. Their corresponding values in 6 M H_2SO_4 + 10% NaCl at 70°C exhibited corrosion rates of 14.304, 92.888 and 40.336 mm/year. These observations are due to the increased agitation of the anionic corrosive species at temperature above room temperature. The slopes of the polarization plots (Figures 2 and 3) are significantly higher than the corresponding values at 30°C ambient temperature. Comparison of the corrosion potentials of B265TiN, B265TiQ, and B265TiA at 70 and 95°C in 2 M H_2SO_4 + 10% NaCl shows visible potential shift in the anodic direction for two reasons (i) increased general surface degeneration in the presence of agitated corrosive species [82], and (ii) greater evolution of oxide complexes on the alloy surface which do not protect the alloy but are by products of chemical reactions at the metal-solution interface. The corresponding values in 6 M H_2SO_4 + 10% NaCl show significant decrease in corrosion potential values for B265TiN, B265TiQ, and B265TiA alloys in the cathodic direction. Nevertheless,

Table 3: Potentiodynamic polarization data for B265TiN, B265TiQ, and B265TiA in 2 M H_2SO_4 + 10% NaCl and 6 M H_2SO_4 + 10% NaCl at 70 and 95°C

B265 Specimen	Temp. (°C)	B265 Corrosion rate (mm/year)	Corrosion current (A)	Corrosion current density (A/cm^2)	Corrosion potential (V)	Polarization resistance, R_p (Ω)	Cathodic potential, B_c	Anodic potential, B_a
2 M H_2SO_4 + 10% NaCl								
N	70	4.979	4.29×10^{-4}	4.29×10^{-4}	−0.516	59.87	−8.343	7.768
Q	70	17.912	1.54×10^{-3}	1.54×10^{-3}	−0.585	16.64	−7.010	2.624
A	70	13.608	1.17×10^{-3}	1.17×10^{-3}	−0.547	21.91	−6.903	3.622
N	95	11.937	1.03×10^{-3}	1.03×10^{-3}	−0.549	26.22	−9.351	2.136
Q	95	20.824	1.80×10^{-3}	1.80×10^{-3}	−0.633	14.31	−8.219	2.497
A	95	15.302	1.32×10^{-3}	1.32×10^{-3}	−0.591	19.48	−5.001	6.012
6 M H_2SO_4 + 10% NaCl								
N	70	16.090	1.39×10^{-3}	1.39×10^{-3}	−0.566	18.52	−3.378	5.904
Q	70	35.812	3.09×10^{-3}	3.09×10^{-3}	−0.589	8.32	−4.703	5.162
A	70	26.485	2.28×10^{-3}	2.28×10^{-3}	−0.604	11.25	−5.693	4.821
N	95	14.304	1.23×10^{-3}	1.23×10^{-3}	−0.465	20.84	−6.363	8.683
Q	95	92.888	8.01×10^{-3}	8.01×10^{-3}	−0.577	3.21	−1.647	8.233
A	95	40.336	3.48×10^{-3}	3.48×10^{-3}	−0.475	7.39	−0.642	4.273

Table 4: Potentiostatic data for B265TiN, B265TiQ, and B265TiA metastable pitting activity and passivation behavior in 2–10 M H_2SO_4 + 10% NaCl at 30°C

H_2SO_4 Conc./ 10% NaCl	Corrosion potential (V)	Metastable pitting initiation potential (V)	Metastable pitting initiation current (A)	Passivation current (A)	Passivation potential (V)	Metastable pitting -passivation potential range (V)	Metastable pitting -passivation current range (A)	Metastable pitting tendency (V)
B265TiN								
10 M	−0.523	−0.430	4.20×10^{-3}	4.72×10^{-5}	−0.010	0.420	4.15×10^{-3}	0.093
8 M	−0.580	−0.450	1.20×10^{-3}	2.08×10^{-5}	−0.070	0.380	1.18×10^{-3}	0.130
6 M	−0.640	−0.410	5.70×10^{-4}	4.46×10^{-5}	−0.130	0.280	5.25×10^{-4}	0.230
4 M	−0.699	−0.460	1.00×10^{-4}	2.01×10^{-5}	−0.190	0.270	7.99×10^{-5}	0.239
2 M	−0.647	−0.370	2.88×10^{-5}	1.79×10^{-5}	−0.190	0.180	1.09×10^{-5}	0.277
B265TiQ								
10 M	−0.491	−0.470	6.40×10^{-3}	4.79×10^{-5}	0.010	0.480	6.35×10^{-3}	0.021
8 M	−0.595	−0.480	1.50×10^{-3}	2.08×10^{-5}	−0.010	0.470	1.48×10^{-3}	0.115
6 M	−0.524	−0.430	3.80×10^{-4}	3.25×10^{-5}	−0.160	0.270	3.48×10^{-4}	0.094
4 M	−0.677	−0.460	1.60×10^{-4}	2.18×10^{-6}	−0.170	0.290	1.58×10^{-4}	0.217
2 M	−0.648	−0.390	2.89×10^{-5}	1.08×10^{-5}	−0.170	0.220	1.81×10^{-5}	0.258
B265TiA								
10 M	−0.461	−0.490	5.90×10^{-3}	5.43×10^{-5}	−0.010	0.480	5.85×10^{-3}	0.029
8 M	−0.467	−0.510	1.30×10^{-3}	2.79×10^{-5}	−0.080	0.430	1.27×10^{-3}	0.043
6 M	−0.568	−0.480	5.30×10^{-4}	4.03×10^{-5}	−0.160	0.320	4.90×10^{-4}	0.088
4 M	−0.661	−0.380	2.31×10^{-5}	4.47×10^{-6}	−0.170	0.210	1.86×10^{-5}	0.281
2 M	−0.631	−0.300	1.37×10^{-5}	3.63×10^{-6}	−0.170	0.130	1.01×10^{-5}	0.331

results show heat treatments, increase in SO_4^{2-} concentration, and temperature significantly influence and decrease the corrosion resistance of B265TiN alloy in aqueous acid-chloride media.

3.2 Potentiostatic studies

Potentiostatic data for B265TiN, B265TiQ, and B265TiA alloys at 30°C in 2–10 M H_2SO_4 + 10% NaCl are displayed

in Table 4, while Table 5 depicts the potentiostatic data for B265TiN, B265TiQ, and B265TiA alloys at 70°C in 2 M H_2SO_4 + 10% NaCl solution. The potentiodynamic plots in Figures 1a–c and 2a displayed significant metastable pitting activity and passivation behavior after anodic polarization. The metastable pitting activity is on account of the nucleation and growth of transient corrosion pits during potential scanning. The pits result from the partial breakdown of TiO_2 on the alloy surface under high electric potential especially at sites of flaws and non-metallic inclusions. The metastable pits which grow due to discharge of the dissolving metallic cations from within the pit for a very short time interval eventually collapse after formation of resistant TiO_2 on the alloy surface at the passive region [83,84]. The potentiodynamic plot configuration shows that metastable pits nucleate at regions with high potentiostatic current values, while time dependent decrease and collapse of the pits occur with the decrease in the potentiostatic current value [85,86]. The decrease in the potentiostatic current value is synonymous with the growth of TiO_2 on the alloy surface until stable passivation is attained. Metastable pit initiation current and potential in Table 4 represents the current (A) and potential (V) value of the estimated region at which transient corrosion pits nucleate [87,88]. Passivation current and potential represents the current (A) and potential value (V) at which TiO_2 repassivates on the Ti alloy surface and sufficiently prevents anodic polarization. Generally, the higher the SO_4^{2-} anion concentration, the higher the metastable pit initiation value due to the electro-reactive nature of the electrolyte at higher concentration. This is also an indication of the extent of vulnerability of the alloy to transient pit formation, resilience of its protective oxide, and capacity to quickly repassivate. At higher SO_4^{2-} concentration (8 M and 10 M H_2SO_4 + 10% NaCl concentration), B265TiN exhibited highest resistance to the formation of metastable pits with values of 4.20×10^{-3} A and 1.20×10^{-3} A (−0.430 V and −0.450 V) compared to B265TiQ and B265TiA at 6.40×10^{-3} A and 1.50×10^{-3} A (−0.470 and −0.480 V), and 5.90×10^{-3} A and 1.30×10^{-3} A (0.490 and −0.510 V), while at lower SO_4^{2-} anion concentrations the values vary among the alloys. B265TiN exhibited the lowest passivation current values in a similar trend to the metastable pit initiation value, signifying a higher tendency to passivate and resist corrosion compared to B265TiQ and B265TiA though the passivation potential values for the alloys at 10 M H_2SO_4 + 10% NaCl concentration are similar. At lower SO_4^{2-} concentrations, the earlier observation did not occur; nevertheless the current and potential at which passivation occurs decreases with decrease in SO_4^{2-}.

Table 5: Potentiostatic data for B265TiN, B265TiQ, and B265TiA metastable pitting activity and passivation behavior in 2 M H_2SO_4 + 10% NaCl at 70°C

Titanium specimen	Corrosion potential (V)	Metastable pitting initiation potential (V)	Metastable pitting initiation current (A)	Passivation current (A)	Passivation potential (V)	Metastable pitting -passivation potential range (V)	Metastable pitting -passivation current range (A)	Metastable pitting tendency (V)
B265TiN	−0.516	−0.350	2.90×10^{-3}	8.36×10^{-5}	0.01	0.360	2.82×10^{-3}	0.170
B265TiQ	−0.585	−0.400	3.30×10^{-3}	1.04×10^{-4}	−0.02	0.380	3.20×10^{-3}	0.190
B265TiA	−0.547	−0.380	3.50×10^{-3}	1.74×10^{-4}	−0.11	0.270	3.33×10^{-3}	0.170

Observation of the metastable pitting current (A) and potential (V) range shows that SO_4^{2-} anion concentration significantly influences the time dependent action of the metastable pitting activity of the alloys. The higher the SO_4^{2-} anion concentration, the higher the metastable pitting range for all the alloys studied. The metastable pitting tendency is the difference in corrosion potential of the alloys and the potential at which metastable pitting initiates. It depicts the extent of anodic polarization on the steel surface before onset of transient localized deterioration of the alloy. The higher the value, the lower the risk to metastable pitting. Generally, the higher the SO_4^{2-} anion concentration, the greater the risk to metastable pitting.

The potentiostatic values for B265TiN, B265TiQ, and B265TiA alloys at 70°C from 2 M H_2SO_4 + 10% NaCl solution show increased temperature of aqueous environments exposes Ti alloy to accelerated corrosion and localized deterioration compared to corrosion at ambient room temperature (30°C). The metastable pit initiation values (current and potential) for the alloys at 70°C are significantly greater than their counterpart values at 30°C in 2 M H_2SO_4 + 10% NaCl solution. At 70°C, the metastable pitting initiation current values for B265TiN, B265TiQ, and B265TiA alloys are 2.9×10^{-3} A, 3.3×10^{-3} A, and 3.5×10^{-3} A compared to 2.88×10^{-5} A, 2.89×10^{-5} A and 1.37×10^{-5} A at 30°C. The corresponding potential values show similar trend. High temperature exposes the alloys to the onset of pit formation due to temporary breakdown and passivation of the TiO_2 on the alloy surface. Similarly, passivation occurred at higher current and lower potentials which signifies weaker or thinner protective oxide at 70°C compared to 30°C. The metastable pitting-passivation potential range values confirm this assertion as they tend to be significantly larger than the corresponding values at 30°C. This shows extended waiting time before collapse of the transient pits or invariable formation of more stable transient pits. The metastable pitting tendency for the alloys at 70°C agrees with the assertion earlier mention for the parameter at 30°C.

3.3 Optical microscopic studies

Optical representative images for B265TiN, B265TiQ, and B265TiA alloys (mag. ×40 and ×100) prior to and subsequently after corrosion test are displayed in Figures 4–11. Figure 4 displays the representative images for B265TiN, B265TiQ, and B265TiA prior to corrosion. Figures 5–7 display the images of B265TiN, B265TiQ, and B265TiA alloys after corrosion test in 2 M H_2SO_4 + 10% NaCl and 10 M H_2SO_4 + 10% NaCl at 30°C, respectively. Figures 8 and 9 show the images for B265TiN, B265TiQ, and B265TiA alloys after corrosion test in 2 M H_2SO_4 + 10% NaCl and 6 M H_2SO_4 + 10% NaCl at 70°C, while Figures 10 and 11 show the images for B265TiN, B265TiQ, and B265TiA alloys after corrosion test in 2 M H_2SO_4 + 10% NaCl and 6 M H_2SO_4 + 10% NaCl at 95°C, respectively. Observation of Figures 5a and 6a and and 7a shows B265TiN, B265TiQ, and B265TiA alloys are highly resistant to corrosion in 2 M H_2SO_4 + 10% NaCl due to the resistant TiO_2 oxide on the alloy surface [89]. The SO_4^{2-} and Cl^- anions from the electrolyte were unable to displace the adsorbed O_2 atoms responsible for the evolution of the protective oxide.

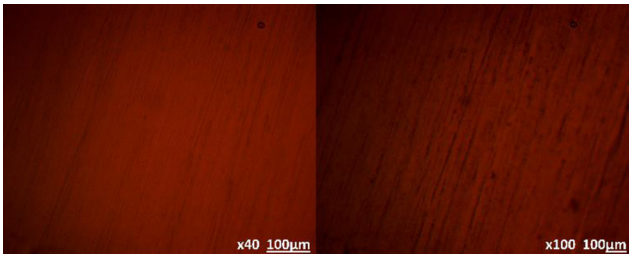

Figure 4: Optical representative images for B265TiN, B265TiQ, and B265TiA alloy before corrosion test.

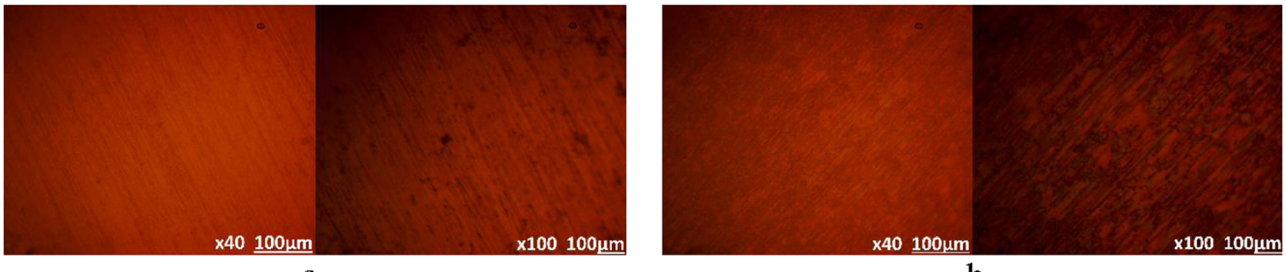

Figure 5: Optical images of B265TiN after corrosion test in (a) 2 M H_2SO_4 + 10% NaCl and (b) 10 M H_2SO_4 + 10% NaCl at 30°C.

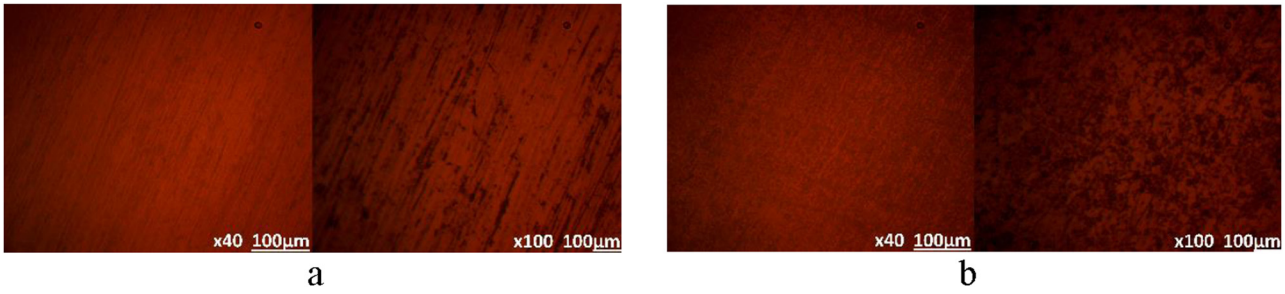

Figure 6: Optical images of B265TiQ after corrosion test in (a) 2 M H_2SO_4 + 10% NaCl and (b) 10 M H_2SO_4 + 10% NaCl at 30°C.

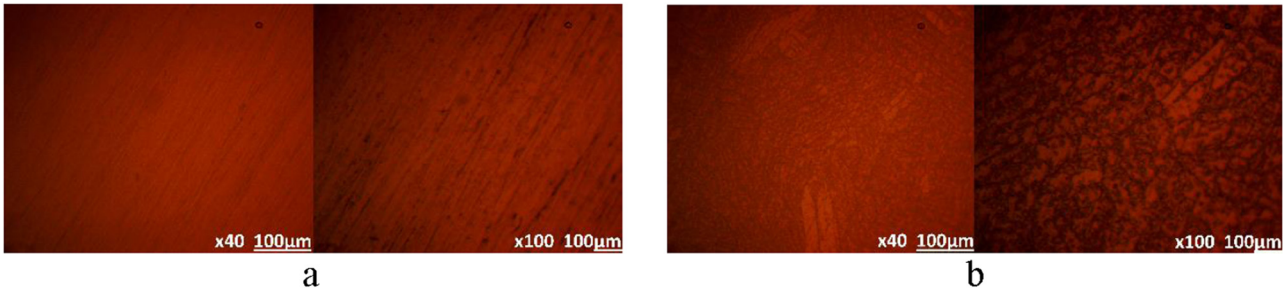

Figure 7: Optical images of B265TiA after corrosion test in (a) 2 M H_2SO_4 + 10% NaCl and (b) 10 M H_2SO_4 + 10% NaCl at 30°C.

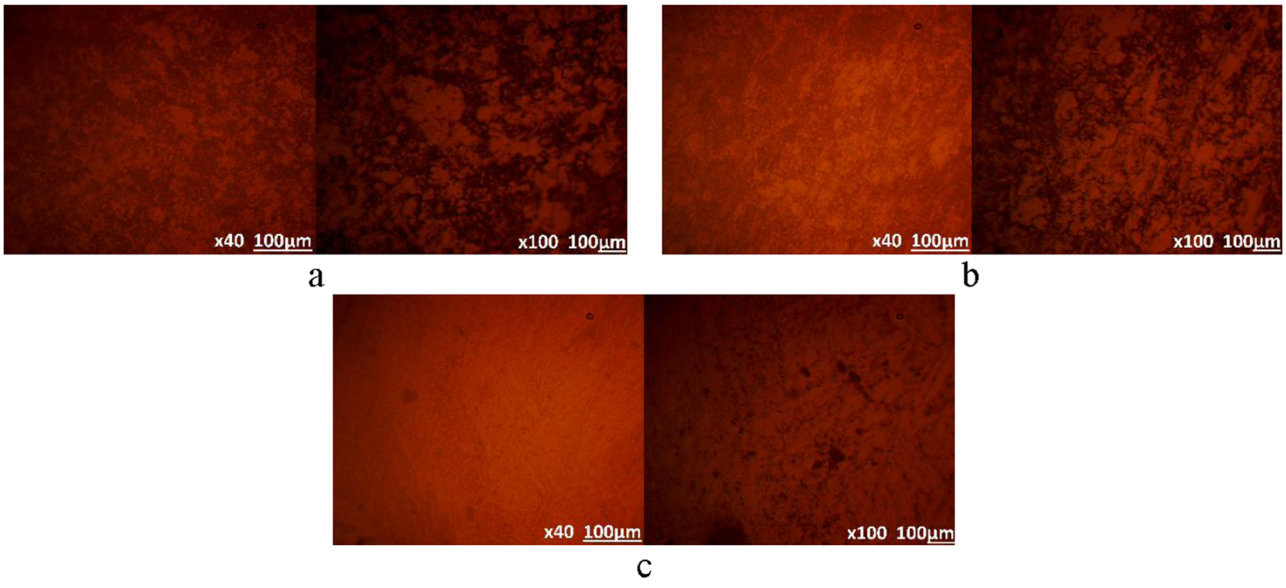

Figure 8: Optical images of (a) B265TiN, (b) B265TiQ, and (c) B265TiA after corrosion test in 2 M H_2SO_4 + 10% NaCl at 70°C.

Hence, the images in Figures 5a and 6a and and 7a are similar to the image in Figure 4 (image before corrosion test) without any sign of significant difference. These statements contrast the observations in Figures 5b, 6b, and 7b, where significant surface deterioration occurred in 10 M H_2SO_4 + 10% NaCl electrolyte. While the surface deterioration on Figure 5b appears marginal, Figure 6b exhibited significant morphological degradation over the entire surface as resistance due to the kinetic barrier of the passive film is unsustainable in the presence of excessive corrosive species and displacement of adsorbed O_2 [90]. The deterioration in Figure 7b appears along the grain/phase boundaries on the alloy. The observed surface deterioration in Figures 6b and 7b is due to the

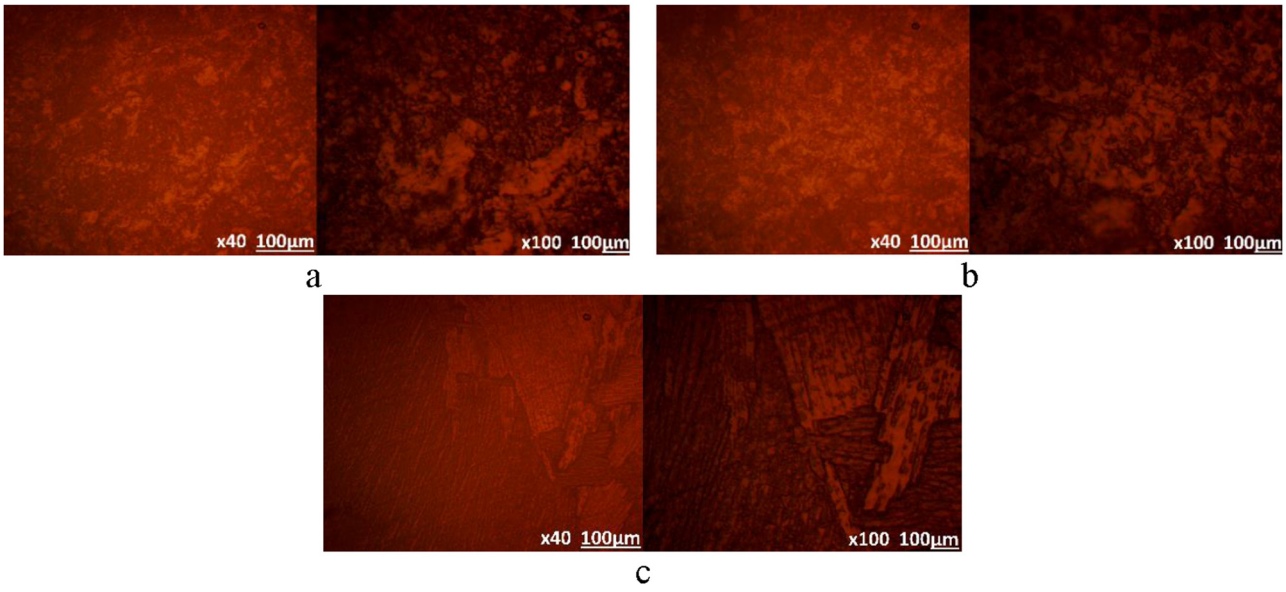

Figure 9: Optical images of (a) B265TiN, (b) B265TiQ, and (c) B265TiA after corrosion test in 6 M H_2SO_4 + 10% NaCl at 70°C.

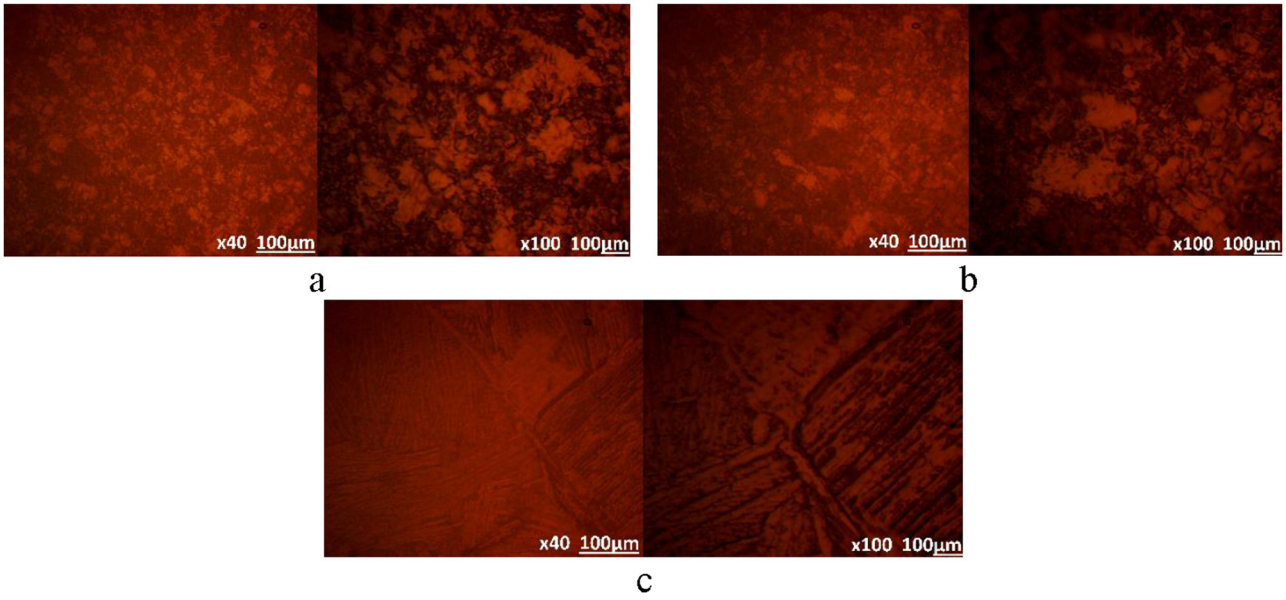

Figure 10: Optical images of (a) B265TiN, (b) B265TiQ, and (c) B265TiA after corrosion test in 2 M H_2SO_4 + 10% NaCl at 95°C.

partial breakage of the protective oxide on the alloy surface which exposes the substrate metal to the debilitating effect of the corrosive anions.

Figures (8a and b) and (9a and b) (from 2 M H_2SO_4 + 10% NaCl and 6 M H_2SO_4 + 10% NaCl at 70°C) exhibited severe morphological deterioration at significantly higher degree compared to the images studied earlier at 30°C. This is due to the entropy of the electrolyte, increased agitation of the corrosive species, and their electrochemical interaction with the alloy surface resulting in the thinning out and eventual breakage of the protective TiO_2. However, the extent of degradation in Figures 8c and 9c contrasts the observation in Figures (8a and b) and (9a and b). B265TiA (Figures 8c and 9c) appears more resistant to corrosion at 70°C compared to B265TiN and B265TiQ (Figures (8a) and (b) and (9a) and (b)). Annealing heat treatment results in metallurgical features where morphological degradation is minimal. This is more

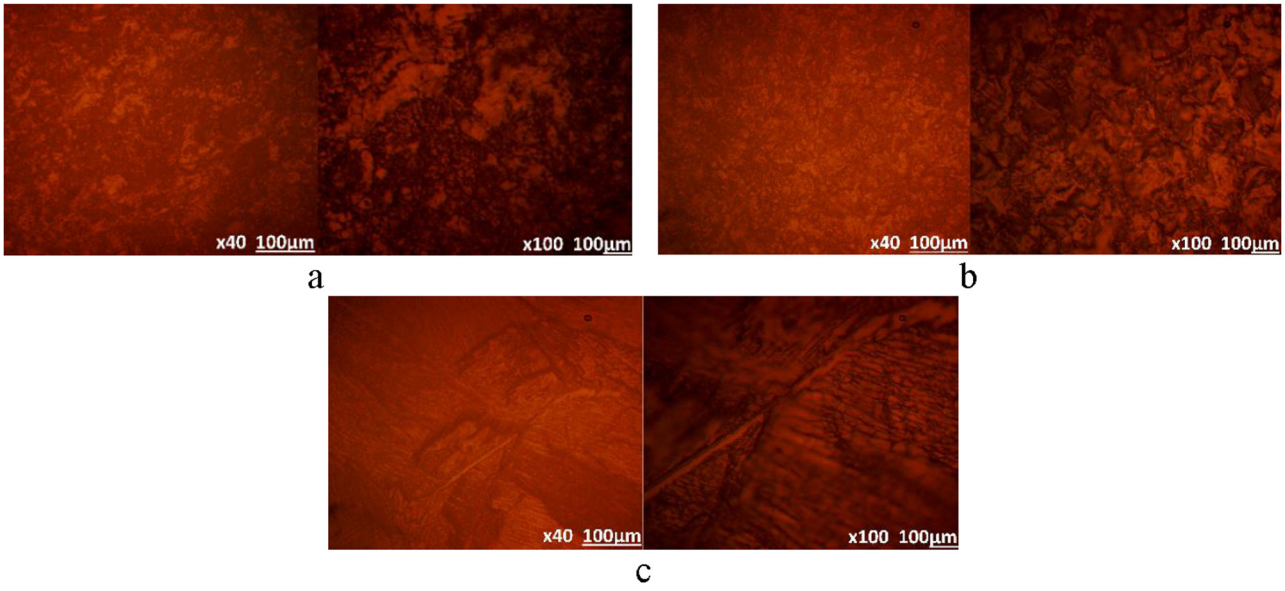

Figure 11: Optical images of (a) B265TiN, (b) B265TiQ, and (c) B265TiA after corrosion test in 6 M H_2SO_4 + 10% NaCl at 95°C.

evident in Figure 9c where the metallurgical phases are visible. Similar observation occurred for the alloy in Figures 10a–c and 11a–c.

3.4 Open circuit potential measurement analysis

The active-passive transition behavior and the thermodynamic properties of B265TiN, B265TiQ, and B265TiA alloys in the acid-chloride media were further studied by OCP measurement and presented in Figures 12–14. Figure 12a and b shows the OCP plots of B265TiN, B265TiQ, and B265TiA alloys in 2 M H_2SO_4 + 10% NaCl solution at 30 and 70°C, while Figures 13(a) and (b) and 14(a) and (b) show the OCP plots of B265TiN, B265TiQ, and B265TiA alloys in 6M H_2SO_4 + 10% NaCl and 6M H_2SO_4 + 10% NaCl solutions, respectively, at 30 and 70°C. Generally, the configuration of the OCP plots in Figures 12a and 13a and and 14a substantially contrast the plots in Figures 12b and 13b and and 14b due to the agitated reaction of the SO_4^{2-} and Cl^- anions with the protective TiO_2 on the Ti alloy surface at the higher temperature. The plots shown in Figures 12a and 13a and and 14a are more thermodynamically stable with limited relative active-passive transition behavior and potential transients due to the stability of the protective oxide on the alloys in the presence of less spontaneous corrosive species. Significant shift to electronegative values at the

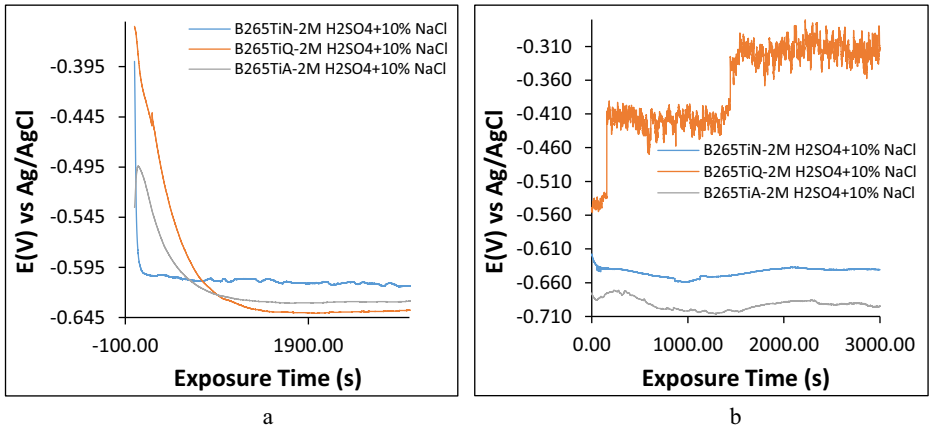

Figure 12: OCP plots of B265TiN, B265TiQ, and B265TiA alloy corrosion in 2 M H_2SO_4 + 10% NaCl solution at (a) 30°C and (b) 70°C.

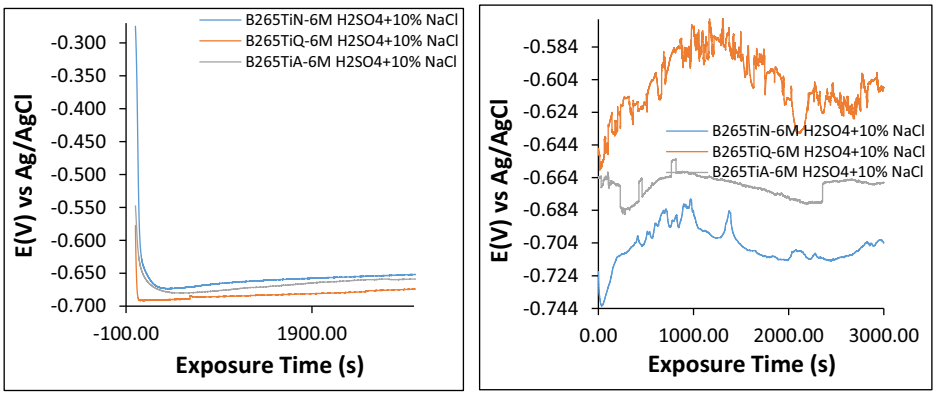

Figure 13: OCP plots of B265TiN, B265TiQ, and B265TiA alloy corrosion in 6 M H_2SO_4 + 10% NaCl solution at (a) 30°C and (b) 70°C.

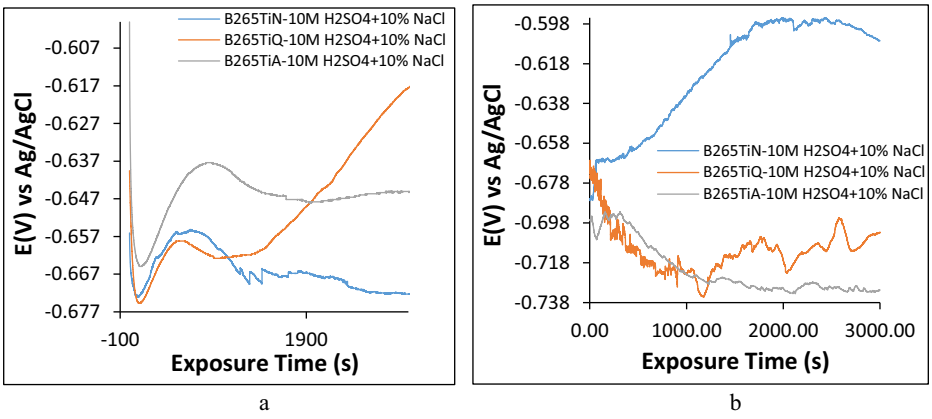

Figure 14: OCP plots of B265TiN, B265TiQ, and B265TiA alloy corrosion in 10 M H_2SO_4 + 10% NaCl solution at (a) 30°C and (b) 70°C.

onset of potential measurement occurred due to the formation of complexes that increases the vulnerability of the alloys to corrosion and prevents the growth of the protective oxide. Observation of these plots show that B265TiN plots (Figures 12a and 13a) were relatively more electropositive throughout in 2 M H_2SO_4 + 10% NaCl and 6 M H_2SO_4 + 10% NaCl up to 3,000 s. In Figure 12a, the plot configuration shows that B265TiN surface is unstable due to its active-passive transition behavior despite having the most resistant protective oxide as evident in its electropositive values. The transition behavior is on account of the growth and breakdown of the protective oxide on the alloy [91–98]. It is also observed (Figure 12a) that the plot configuration of B265TiA generally remained stable with respect to exposure time from 965.61 s (−0.624 V) due to the stability of its oxide.

In Figure 14a, the high concentration of the SO_4^{2-} anions (10 M concentration) coupled with the Cl^- anions present results in significant active-passive transition behavior of the alloys. B265TiQ plot significantly progressed in the electropositive direction in the presence of the corrosive anions. Due to the strong affinity of the alloy for O_2, its protective oxide continues to grow until a peak threshold value of 3,000 s (−0.617 V). Within the same diagram (Figure 14a), B265TiN after undergoing active-passive transition behavior before attaining relative stability at 1,422.01 s (−0.670 V) till 3,000 s. It must be noted that OCP plots in Figure 12a for B265TiN, B265TiQ, and B265TiA generally attained pseudo stability at around −0.600 V (90.8 s), −0.639 V (1488.81 s), and −0.623 V (942.01 s), while the corresponding plots in Figure 13a attained pseudo stability at −0.676 V (278.2 s) and −0.691 V (59.4 s), and peaked at −0.651 V, −0.650 V, and −0.640 V (3,000 s), respectively. This shows that the titanium alloys are more prone to electrochemical reaction responsible for corrosion induced by higher concentrations of SO_4^{2-} anions in the electrolyte. This observation contrasts the plot configuration in Figure 14a where they attained

pseudo stable states after extended active-passive transition behavior. After an initial but brief sharp decrease to more electronegative potentials, the plots generally progressed thereafter to electropositive values beginning at −0.655 V (645.41 s), −0.658 V (544.4 s), and −0.637 V (853.81 s) for B265TiN, B265TiQ, and B265TiA, respectively. While the OCP plots for B265TiN and B265TiA attained marginal thermodynamic stability till 3,000 s, the plots for B265TiQ continues to progress to higher electropositive potentials due to growth of its protective oxide.

The plots in Figures 12b and 13b and and 14b significantly vary from their counterparts in Figures 12a, 13a, and 14a as earlier mentioned. While B265TiN and B265TiA in Figure 12b were generally thermodynamically stable with respect to exposure time, their OCP plots were more electronegative than their counterparts in Figure 12a due to reasons mentioned earlier. High temperature exposes the alloy to accelerated deterioration of the alloy surface. However, the behavior of B265TiQ (Figure 12b) contrast the behavior of the other alloys despite significant potential transients and active-passive transition behaviors. The plot of the alloy visibly progressed to electropositive values signifying the evolution of a resistant protective oxide on the alloy exterior. The potential transients show that the protective oxide is highly reactive in the presence of the corrosive species and not thermodynamically stable despite being sufficient and thick enough to reduce the reaction processes causing corrosion [99,100]. In Figure 13b, the protective oxide on B265TiQ alloys proves to be the most resistant being the most electropositive. Its potential initiated at 0.646 V (0 s) and attained an approximate peak electropositive potential at 1251.21 s (−0.579 V) before marginally decreasing to −0.609 V at 3,000 s. This behavior occurred at 6 M SO_4^{2-} anion concentration compared to 2 M SO_4^{2-} anion concentration in Figure 12b.

It is observed that the potential transient for B265TiQ in Figure 13b is much widely spaced compared to Figure 12b due to significant failure and repassivation of the protective oxide [101]. At 6 M SO_4^{2-} concentration, the OCP plot of B265TiQ is more electronegative compared to its counterpart in Figure 12b. B265TiN and B265TiA alloys in Figure 13b are more electronegative than their counterparts in Figure 12b. B265TiN proves to be the most reactive and vulnerable to corrosion in Figure 13b with final potential of −0.704 V at 3,000 s. Its counterpart in Figure 12b has a final potential value of −0.647 V. In Figure 14b, B265TiQ and B265TiA exhibited a higher tendency to corrode. Their corrosion potential initiated at −0.670 V and −0.697 V (0 s) and progressively decreased to electronegative values associated with higher vulnerability to corrosion. While the electronegative shift was instantaneous for B265TiQ, prolonged decline occurred for B265TiA at 277.4 s (−0.695 V). B265TiA plot achieved relative stability at 1,267 s (−0.728 V) till 3,000 s. At 1,200 s (−0.733 V), the protective oxide on B265TiQ stabilized and begins to grow as evident on its plot configuration in Figure 14b. However, the active-passive transition behavior of the plot shows that the oxide is not stable due to the reactive complexes it forms with the corrosive anions. In contrast to it performance in Figures 12b and 13b, B265TiN exhibited strong resistance to the corrosive attack of SO_4^{2-} and Cl^- in Figure 14b. The OCP plot for B265TiN initiated at −0.686 V and significantly progressed to −0.597 V at 1,880.42 s where it achieved relative stability due to growth and thickening of its protective oxide till −0.598 V (2603.82 s). Beyond this point there was a marginal decrease till 3,000 s.

4 Conclusion

Untreated B265 titanium alloy exhibited strong resistance to general corrosion at room and elevated temperatures when compared with the quenched and annealed alloy. The quenched alloy was the most vulnerable to corrosion. The potentiodynamic polarization behavior of the alloy shows cathodic reaction mechanisms dominated the redox electrochemical process. The surface morphology of the untreated and heat-treated titanium alloys displayed strong resistance to corrosive degradation in low electrolyte concentration at room temperature. However, from the highest electrolyte concentration, significant general surface degradation was visible for quenched titanium alloy and degradation along grain boundaries for annealed titanium alloy. The extent of degradation was significantly higher in electrolyte at high temperature. The alloys displayed significant metastable pitting activity and passivation behavior with the untreated steel being the most resistant to metastable pits formation. Plots from open circuit potential measurement depict untreated titanium alloy was generally the least vulnerable to corrosion with stable oxide formation at room temperature and comparative low concentration of the electrolyte. Quenched titanium alloy exhibited the least vulnerability to corrosion with highly unstable oxide at higher temperature of the electrolyte.

Acknowledgement: The authors acknowledge the support of Covenant University towards the execution and success of this research.

Conflict of interest: Author declare no conflict of interest.

References

[1] Lütjering G, Williams JC. Beta alloys. Berlin: Springer; 2007.
[2] Adam G, Zhang DL, Liang J, Macrae I. A novel process for lowering the cost of titanium. AMR. 2007;147(52):29–30. doi: 10.4028/www.scientific.net/amr.29-30.147.
[3] Fattah-Alhosseini A, Vakili-Azghandi M, Sheikhi M, Keshavarz MK. Passive and electrochemical response of friction stir processed pure titanium. J Alloys Compd. 2017;704:499–508.
[4] Boyer RR. An overview on the use of titanium in the aerospace industry. Mater Sci Eng. 1996;A213:103–14.
[5] Yamada M. An overview on the development of titanium alloys for non-aerospace application in Japan. Mater Sci Eng. 1996;A213:8–15.
[6] Yaya K, Khelfaoui Y, Malki B, Kerkar M. Numerical simulations study of the localized corrosion resistance of AISI 316l stainless steel and pure titanium in a simulated body fluid environment. Corros Sci. 2011;53:3309–14.
[7] Khan MA, Williams RL, Williams DF. *In-vitro* corrosion and wear of titanium alloys in the biological environment. Biomaterials. 1996;17:2117–26.
[8] Barril S, Mischler S, Landolt D. Influence of fretting regimes on the tribocorrosion behaviour of Ti6Al4V in 0.9 wt% sodium chloride solution. Wear. 2004;254:963–72.
[9] Duisabeau L, Combrade P, Forest B. Environmental effect on fretting of metallic materials for orthopaedic implants. Wear. 2004;256:805–16.
[10] Shevchenko N, Pham MT, Maitz MF. Studies of surface modified NiTi alloy. Appl Surf Sci. 2004;235:126–31.
[11] Johansson BI, Bergman B. Corrosion of titanium and amalgam couples: Effect of fluoride, area, size, surface preparation and fabrication procedures. Dent Mater. 1995;11:41–6.
[12] Long M, Rack HJ. Titanium alloys in total joint replacement – a materials science perspective. Biomaterials. 1998;19:1621–39.
[13] Leyens C, Peters M. Titanium and titanium alloys: fundamentals and applications. New York: Wiley; 2003.
[14] Schutz RW. Defining the corrosion performance window grade 28 Titanium. San Diego, California: NACE Corrosion; 2003.
[15] Thomas R. Titanium in the geothermal industry. Geothermics. 2003;32:679–87.
[16] Contu F, Elsener B, Böhni H. Serum effect on the electrochemical behaviour of titanium, Ti6Al4V and Ti6Al7Nb alloys in sulphuric acid and sodium hydroxide. Corros Sci. 2004;46:2241–54.
[17] Narayanan R, Seshadri SK. Point defect model and corrosion of anodic oxide coatings on Ti–6Al–4V. Corros Sci. 2008;50:1521–9.
[18] Tamilselvi S, Raman V, Rajendran N. Evaluation of corrosion behavior of surface modified Ti–6Al–4V ELI alloy in hanks solution. J Appl Electrochem. 2010;40:285–93.
[19] Kaminaka H, Abe M, Matsumoto S, Kimura K, Kamio H. Characteristics and applications of high corrosion resistant titanium alloys. Nippon Steel & Sumitomo Metal Technical Report No. 106; 2004. https://www.nipponsteel.com/en/tech/report/nssmc/pdf/106-07.pdf.
[20] Krawiec H, Vignal V, Loch J, Erazmus-Vignal P. Influence of plastic deformation on the microstructure and corrosion behaviour of Ti–10Mo–4Zr and Ti–6Al–4V alloys in the Ringer's solution at 37°C. Corros Sci. 2015;96:160–70.
[21] Browne M, Gregson PJ. Surface modification of titanium alloy implants. Biomaterials. 1994;15:894–8.
[22] Ban S, Hasegaw J, Maruno S. Electrochemical corrosion behaviour of hydroxyapatite-glass-titanium composite. Biomaterials. 1991;12:205–9.
[23] Khan MA, Williams RL, Williams DF. Conjoint corrosion and wear in titanium alloys. Biomaterials. 1991;20:765–72.
[24] Fekry AM, El-Sherif RM. Electrochemical corrosion behavior of magnesium and titanium alloys in simulated body fluid. Electrochim Acta. 2009;54:7280–5.
[25] Cheng Y, Hu J, Zhang C, Wang Z, Hao Y, Gao B. Corrosion behavior of novel Ti-24Nb-4Zr-7.9Sn alloy for dental implant application *in vitro*. J Biomed Mater Res Part B. 2013;101B:287–94.
[26] Peláz-Abellán E, Rocha-Sousa L, Műller WD, Guastaldi AC. Electrochemical stability of anodic titanium oxide films grown at potentials higher than 3V in a simulated physiological solution. Corros Sci. 2007;49:1645–55.
[27] Mansfeld F, Tsai R, Shih H, Litrle B, Ray R, Wagne P. An electrochemical and surface analytical study of stainless steels and titanium exposed to natural seawater. Corros Sci. 1992;33:445–56.
[28] Laboulais JN, Matab AA, Borrásb VA, Muñoza AI. Electrochemical characterization and passivation behaviour of new beta-titanium alloys (Ti35Nb10Ta-xFe). Electrochim Acta. 2017;227:410–8.
[29] Simka W, Kaczmarek M, Baron-Wiecheć A, Nawrat G, Marciniak J, Żak J. Electropolishing and passivation of NiTi shape memory alloy. Electrochim Acta. 2010;55:2437–41.
[30] El Hadad AA, Barranco V, Jimenez-Morales A, Hickman GJ, Galván JC, Perry CC. Triethylphosphite as a network forming agent enhances *in vitro* biocompatibility and corrosion protection of hybrid organic–inorganic sol–gel coatings for Ti6Al4V alloys. J Mater Chem B. 2014;2:7955–63.
[31] Çomakli O, Yetim F. Tribological and electrochemical behavior of Ag_2O/ZnO/NiO nanocomposite coating on commercial pure titanium for biomedical applications. Ind Lubr Tribol. 2019;71:1166–76.
[32] Çomakli O, Yazici M, Yetim T, Yetim AF, Çelik A. Effect of Ti amount on wear and corrosion properties of Ti-doped Al_2O_3 nanocomposite ceramic coated CP titanium implant material. Ceram Int. 2018;44:7421–8.
[33] Çomakli O, Yazici M, Kovaci H, Yetim T, Yetim AF, Çelik A. Tribological and electrochemical properties of TiO_2 films

produced on Cp-Ti by sol-gel and SILAR in bio-simulated environment. Surf Coat Technol. 2018;352:513–21.
[34] Loto CA, Loto CA, Joseph OO, Loto RT. Adsorption and inhibitive properties of Camellia Sinensis for aluminium alloy in HCl. Int J Elect Sci. 2014;9(7):3637–49.
[35] Loto CA, Loto CA, Loto RT, Popoola API. Synergistic effect of tobacco and kola tree extracts on the corrosion inhibition of mild steel in acid chloride. Int J Elect Sci. 2011;6(9):3830–43.
[36] Nabhani M, Razavi RS, Barekat M. Corrosion study of laser cladded Ti–6Al–4V alloy in different corrosive environments. Eng Fail Anal. 2019;97:234–41.
[37] Al-Mayouf AM, Al-Swayih AA, Al-Mobarak NA. Effect of potential on the corrosion behavior of a new titanium alloy for dental implant applications in fluoride media. Mater Corros. 2004;55:88–94.
[38] Chambers B, Venkatesh A, Mishael S. Performance of tantalum-surface alloy on stainless steel and multiple corrosion resistant alloys in laboratory evaluation of deep well acidizing environments. Houston: NACE Corrosion; 2011.
[39] Su Z, Bühl M, Zhou W. Dissociation of water during formation of anodic aluminum oxide. J Am Chem Soc. 2009;131:8697.
[40] Kane RD, Srinivasan S, Craig B, Yap KM. A comprehensive study of Ti alloys for high pressure (HPHT) wells. Dallas: NACE Corrosion; 2015.
[41] Schutz RW, Jena BC. Sour service test qualification of a new high-strength Ti alloy-UNS R55400. Dallas: NACE Corrosion; 2015.
[42] Diamanti MV, Codeluppi S, Cordioli A, Pedeferri MP. Effect of thermal oxidation on titanium oxides' characteristics. J Exp Nanosci. 2009;4(4):365–72.
[43] Davis JR. Alloying – understanding the basics. ASM International; 2003. p. 425.
[44] Vaughan J, Alfantazi A. Corrosion of titanium and its alloys in sulfuric acid in the presence of chlorides. J Electrochem Soc. 2006;153(1):B6–B12.
[45] Jaquez-Muñoz J, Gaona-Tiburcio C, Lira-Martinez A, Zambrano-Robledo P, Maldonado-Bandala E, Samaniego-Gamez O, et al. Susceptibility to pitting corrosion of Ti-CP_2, Ti-6Al-2Sn-4Zr-2Mo, and Ti–6Al–4V alloys for aeronautical applications. Metals. 2021;11(7):1002.
[46] Yang X, Dong X, Li W, Feng W, Xu Y. Effect of solution and aging treatments on corrosion performance of laser solid formed Ti–6Al–4V alloy in a 3.5 wt% NaCl solution. J Mater Res Techn. 2020;9(2):1559–68.
[47] Lipsitt HA. Titanium aluminides – an overview. Materials Research Society Symposium Proceedings. Vol. 39; 1984. p. 351–65.
[48] Banerjee D. Ti_3Al and its alloys. Intermetallic compounds, principles and practice. Vol. 2. Chichester, England: John Wiley; 1995. p. 91–131.
[49] Huang S, Chesnutt JC. TiAl and its alloys. Intermetallic compounds, principles and practice. Vol. 2. Chichester, England: John Wiley; 1995. p. 73–90.
[50] Yamaguchi M, Inui H. Al_3Ti and its L12 variation. Intermetallic compounds, principles and practice. Vol. 2. Chichester, England: John Wiley & Sons Ltd; 1995. p. 73–90.
[51] Djanarthany S, Viala J-C, Bouix J. An overview of monolithic titanium aluminides based on Ti_3Al and TiAl. Mats Chem Phys. 2001;72(3):301–19.
[52] Yue TM, Yu JK, Mei Z, Man HC. Excimer laser surface treatment of Ti–6Al–4V alloy for corrosion resistance enhancement. Mater Lett. 2002;52:206–12.
[53] Blanco-Pinzon C, Liu Z, Voisey K, Bonilla FA, Skeldo P, Thompson GE, et al. Excimer laser surface alloying of titanium with nickel and palladium for increased corrosion resistance. Corros Sci. 2005;47:1251–69.
[54] Krýsa J, Mráz R, Roušar I. The corrosion rate of titanium in H_2SO_4. Mats. Chem Phys. 1997;48(1):64–7.
[55] Bodunrin MO, Chown LH, Merwe JW, Alaneme KK. Corrosion behaviour of Ti-Al-xV-yFe experimental alloys in 3.5 wt% NaCl and 3.5 M H_2SO_4. Mater Corros. 2018;69(6):770–80.
[56] Mogoda A, Ahmad Y, Badawy W. Corrosion behaviour of Ti–6Al–4V alloy in concentrated hydrochloric and sulphuric acids. J Appl Electrochem. 2004;34:873–8.
[57] Chih CY, Chen JR, Tsai WT. Selective dissolution of Ti–6Al–4V titanium alloy in mixed HCl + H_2SO_4 solution. Atlanta, Georgia: NACE Corrosion; 2009.
[58] Falodun OE, Obadele BA, Oke SR, Maja ME, Ige OO, Olubambi PA. Corrosion behaviour of spark plasma sintered Ti–6Al–4V with Nano-TiN addition in different media. IEEE 9th International Conference on Mechanical and Intelligent Manufacturing Technologies; 2018. p. 60–3
[59] Ciszak C, Popa L, Brossard J-M, Monceau D, Chevalier S. NaCl induced corrosion of Ti–6Al–4V alloy at high temperature. Corros Sci. 2016;110:91–104.
[60] Yang J, Yang H, Yu H, Wang Z, Zeng X. Corrosion behavior of additive manufactured Ti–6Al–4V alloy in NaCl solution. Metall Mater Trans A. 2017;48:3583–93.
[61] Abdeen DH, Palmer BR. Corrosion evaluation of Ti–6Al–4V parts produced with electron beam melting machine. Rapid Prototyp J. 2017;2(22):322–9.
[62] Dai N, Zhang LC, Zhang J, Chen Q, Wu M. Corrosion behavior of selective laser melted Ti–6Al–4V alloy in NaCl solution. Corros Sci. 2017;102:484–9.
[63] Ramiresand I, Guastaldi AC. Electrochemical study of the corrosion of TiPd and Ti–6Al–4V electrodes in sodium chloride solutions. Biomecánica. 2001;9(1):61–5.
[64] Atapour M, Pilchak A, Frankel GS, Williams JC, Fathi MH, Shamanian M. Corrosion behavior of Ti–6Al–4V with different thermomechanical treatments and microstructures. Corrosion. 2010;66(6):065004–9.
[65] ASTM G59-97. Standard test method for conducting potentiodynamic polarization resistance measurements; 2014. http://www.astm.org/Standards/G31 [Accessed 06/04/21].
[66] ASTM G1-03. Standard practice for preparing, cleaning, and evaluating corrosion test specimens; 2011. http://www.astm.org/Standards/G1 [Accessed 06/04/21].
[67] ASTM G102-89. Standard practice for calculation of corrosion rates and related information from electrochemical measurements; 2015. http://www.astm.org/Standards/G102.htm [Accessed 06/04/21].
[68] Basics of corrosion measurements. http://www.che.sc.edu/faculty/popov/drbnp/ECHE789b/Corrosion%20Measurements.pdf [Accessed 06/04/21].
[69] Loto RT, Loto CA, Popoola API, Kupolati W. Corrosion inhibition effect of N, N-diphenylthiourea on the electrochemical

characteristics of mild steel in dilute acidic environments. J Chem Soc Pakistan. 2016;38(2):222–33.
[70] Zhang XD, Bonniwell P, Fraser HL, Baeslack III WA, Evans DJ, Ginter T, et al. Effect of heat treatment and silicon addition on the microstructure development of Ti–6Al–2Cr–2Mo–2Sn–2Zr alloy. Mater Sci Eng A. 2003;343(1–2):210–26.
[71] Raj B, Mudali UK. Materials development and corrosion problems in nuclear fuel reprocessing plants. Prog Nucl Energy. 2006;48(4):283–313.
[72] Cotolan N, Pop A, Marconi D, Ponta O, Muresan LM. Corrosion behaviour of TiO_2-coated Ti-6Al-7Nb surfaces obtained by anodic oxidation in sulphuric or acetic acid. Mater Corros. 2015;66(7):635–42.
[73] Shu YH, Wang FH, Wu WT. Corrosion behavior of Ti60 alloy coated with a solid NaCl deposit in O_2 plus water vapor at 500–700°C. Oxid Met. 1999;52:463–73.
[74] Shu YH, Wang F, Wu WT. Synergistic effect of NaCl and water vapor on the corrosion of 1Cr-11Ni-2W-2Mo-V steel at 500–700°C. Oxid Met. 1999;51:97–110.
[75] Shu YH, Wang FH, Wu WT. Corrosion behavior of pure Cr with a solid NaCl deposit in O_2 plus water vapour. Oxid Met. 2000;54:457–71.
[76] Dini C, Costa RC, Sukotjo C, Takoudis CG, Mathew MT, Barão VAR. Progression of bio-tribocorrosion in implant dentistry, Front. Mech Eng. 2020;6:1–14.
[77] Zhang L, Chen L. A review on biomedical titanium alloys: Recent progress and prospect. Adv Eng Mater. 2019;21:1801215.
[78] Noronha Oliveira M, Schunemann WVH, Mathew MT, Henriques B, Magini RS, Teughels W, et al. Can degradation products released from dental implants affect peri-implant tissues? J Periodontal Res. 2017;6:1–11.
[79] Mombelli A, Hashim D, Cionca N. What is the impact of titanium particles and biocorrosion on implant survival and complications? A critical review. Clin Oral Implant Res. 2018;29(18):37–53.
[80] Zhang LC, Chen LY, Wang L. Surface modification of titanium and titanium alloys: technologies, developments, and future interests. Adv Eng Mater. 2020;22:1901258.
[81] Bourikas K, Hiemstra T, Van Riemsdijk WH. Ion pair formation and primary charging behavior of titanium oxide (Anatase and Rutile). Langmuir. 2001;17:749–56.
[82] Mischler S. Triboelectrochemical techniques and interpretation methods in tribocorrosion: a comparative evaluation. Tribol Int. 2008;41:573–83.
[83] He X. Electrochemical behavior and passivity of titanium grades 7 and 29 under immersion conditions, U.S. Nuclear Regulatory Commission Contract NRC–02–07–006. San Antonio, Texas: Center for Nuclear Waste Regulatory Analyses; 2011.
[84] Pistorius PC, Burstein GT. Metastable pitting corrosion of stainless steel and the transition to stability. Philos Trans Royal Soc. 1992;341:531–59. doi: 10.1098/rsta.1992.0114.
[85] Tian W, Du N, Li S, Chen S, Wu Q. Metastable pitting corrosion of 304 stainless steel in 3.5% NaCl solution. Corros Sci. 2014;85:372–9.
[86] Cheng YF, Wilmott M, Luo JL. Transition criterion of metastable pitting towards stability for carbon steel in chloride solutions. Brit Corr J. 1999;34(4):280–4.
[87] Loto RT. Comparative study of the pitting corrosion resistance, passivation behavior and metastable pitting activity of NO7718, NO7208 and 439L super alloys in chloride/sulphate media. J Mater Res Technol. 2019;8(1):623–9.
[88] Loto RT, Loto CA. Comparative assessment of the pitting corrosion resistance and passivation behaviour of 439L ferritic and 904L austenitic stainless steels for application in extreme process environments. J Bio Tribo Corr. 2019;5:57. doi: 10.1007/s40735-019-0249-1.
[89] Gittens RA, Scheideler L, Rupp F, Hyzy SL, Geis-Gerstorfer J, Schwartz Z, et al. A review on the wettability of dental implant surfaces II: Biological and clinical aspects. Acta Biomater. 2014;10:2907–18.
[90] Virtanen S. Degradation of Titanium and Its Alloys. In: Eliaz N, editor. Degradation of implant materials. New York, NY: Springer; 2012. doi: 10.1007/978-1-4614-3942-4_2.
[91] Brauns E, Schwenk W. Contribution to the kinetics of pitting corrosion on passive chromium-nickel steels. Mater Corros. 1961;12:73–80.
[92] Schwenk W. Theory of stainless steel pitting. Corrosion. 1964;20(4):129t–137t.
[93] Bond AP, Lizlovs AZ. Anodic polarization of austenitic stainless steels in chloride media. J Electrochem Soc. 1968;115(11):1130.
[94] Forchhammer P, Engell HJ. Investigations into pitting corrosion on passive austenitic chromium-nickel steels in neutral chloride solutions. Mater Corros. 1969;20:1–12.
[95] Hisamatsu Y, Yoshii T, Matsumra Y. Localized corrosion, NACE-3. Houston: NACE; 1974. p. 427.
[96] Sato N. Anodic breakdown of passive films on metals. J Electrochem Soc. 1982;129:255–9.
[97] Williams DE, Fleischmann M, Stewart J, Brooks T. Some characteristics of the initiation phase of pitting corrosion of stainless steel. Mater Sci Forum. 1986;8:151–66.
[98] Frankel GS, Stockert L, Hunkeler F, Böhni H. Metastable pitting of stainless steel. Corrosion. 1987;43:429–36.
[99] Jaquez-Munoz JM, Gaona-Tiburcio C, Cabral-Miramontes J, Nieves-Mendoza D, Maldonado-Bandala E, Olguin-Coca J, et al. Electrochemical noise analysis of the corrosion of titanium alloys in NaCl and H_2SO_4 solutions. Metals. 2021;11:105.
[100] Cui J, Yu D, Long Z, Xi B, He X, Pei Y. Application of electrochemical noise (EN) technology to evaluate the passivation performances of adsorption and film-forming type corrosion inhibitors. J Electroanal Chem. 2019;855:113584.
[101] Pistorius PC, Burstein GT. Metastable pitting corrosion of stainless steel and the transition to stability. Philos Trans Royal Soc. 1992;341:531–59. doi: 10.1098/rsta.1992.0114.